A surrogate model for the economic evaluation of renewable hydrogen production from biomass feedstocks via supercritical water gasification

Sarah Rodgers [a], Alexander Bowler [b], Laura Wells [c], Chai Siah Lee [d], Martin Hayes [e], Stephen Poulston [f], Edward Lester [d], Fanran Meng [g], Jon McKechnie [a], Alex Conradie [h,*]

[a] Sustainable Process Technologies Research Group, Faculty of Engineering, University of Nottingham, Nottingham, NG7 2RD, UK

[b] School of Food Science and Nutrition, University of Leeds, Woodhouse Ln., Leeds, LS2 9JT, UK

[c] Johnson Matthey, 5 Farringdon St, London, EC4A 4AB, UK

[d] Advanced Materials Research Group, Faculty of Engineering, University of Nottingham, NG7 2RD, UK

[e] Johnson Matthey, 28 Cambridge Science Park, Milton Road, Cambridge, CB4 0FP, UK

[f] Johnson Matthey, Blounts Court Road, Sonning Common, Reading, RG4 9NH, UK

[g] Chemical & Biological Engineering, University of Sheffield, Mappin Street, Sheffield, S1 3JD, UK

[h] The Manufacturing Futures Laboratory, Department of Biochemical Engineering, University College London, Gower Street, London, WC1E 6BT, UK

HIGHLIGHTS

- A techno-economic surrogate model for supercritical water gasification is created.
- Model predicts the LCOH for different biomass compositions, scales, and locations.
- RF, SVR, and ANN algorithms were compared for the surrogate model.
- ANNs achieved the highest prediction accuracy during cross-validation.
- Final model is published to facilitate early-stage feedstock evaluation.

GRAPHICAL ABSTRACT
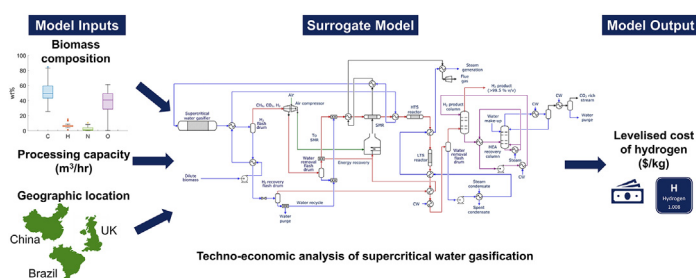
Techno-economic analysis of supercritical water gasification

ARTICLE INFO

ABSTRACT

Supercritical water gasification is a promising technology for renewable hydrogen production from high moisture content biomass. This work produces a machine learning surrogate model to predict the Levelised Cost of Hydrogen over a range of biomass compositions, processing capacities, and geographic locations. The model is published to

facilitate early-stage economic analysis (doi.org/10.6084/m9.figshare.22811066). A process simulation using the Gibbs reactor provided the training data using 40 biomass compositions, five processing capacities (10–200 m^3/h), and three geographic locations (China, Brazil, UK). The levelised costs ranged between 3.81 and 18.72 \$/kg$_{H2}$ across the considered parameter combinations. Heat and electricity integration resulted in low process emissions averaging 0.46 kgCO$_2$eq/GJ$_{H2}$ (China and Brazil), and 0.37 kgCO$_2$eq/GJ$_{H2}$ (UK). Artificial neural networks were most accurate when compared to random forests and support vector regression for the surrogate model during cross-validation, achieving an accuracy of MAPE: <4.6%, RMSE: <0.39, and R^2: >0.99 on the test set.

Abbreviations

AD	Anaerobic Digestion
ANN	Artificial Neural Network
CCS	Carbon Capture and Storage
COD	Chemical Oxygen Demand
EIA	Energy Information Administration
GHG	Greenhouse Gas
HHV	Higher Heating Value
HTS	High Temperature Shift
LCA	Life Cycle Assessment
LCOH	Levelised Cost of Hydrogen
LTS	Low Temperature Shift
MAPE	Mean Absolute Percentage Error
MEA	Monoethanolamine
ML	Machine Learning
MSP	Minimum Selling Price
RF	Random Forests
RMO	Ratio of Moles of Oxygen
RMSE	Route Mean Squared Error
SCWG	Supercritical Water Gasification
SHAP	SHapley Additive exPlanation
SMR	Steam Methane Reforming
SVR	Support Vector Regression
TEA	Techno-Economic Analysis

1. Introduction

Supercritical Water Gasification (SCWG) combines thermal decomposition and reforming by using supercritical water as the solvation and reaction medium, thereby converting various biomass feedstocks to syngas (H$_2$, CH$_4$, CO$_2$ and CO) whilst minimising char formation. SCWG provides advantages for processing wet feedstocks over other bioenergy generation approaches (e.g. direct combustion and conventional gasification) such as energy savings by avoiding the need to pre-dry the feedstock, lower operating temperatures, shorter reaction times and tuneable gas compositions [1].

The past decade has seen an increased focus on experimental investigations of hydrogen production via SCWG using various types of plant-based biomass feedstocks, such as sugarcane bagasse, stillage, and black liquor [2]. To understand the economic potential of a feedstock it is necessary to conduct a Techno-Economic Analysis (TEA). Several TEAs have been undertaken using SCWG for renewable hydrogen production from specific feedstocks including the valorisation of digested sewage sludge [3], black liquor [4], and soybean straw [5]. However, detailed TEAs are time consuming and require engineering knowledge and economic modelling expertise [6]. This hinders the creation of TEA models by non-experts i.e. experimentalists and industrialists. Moreover, TEA models are most often specific to a particular process, scale, feedstock, and cost base, limiting the ability to generalise effectively from existing models. Without understanding how operating conditions, feedstock sources, and cost considerations impact on the overall investment case, targeted experimental research is impeded, which is detrimental to subsequent commercialisation. Therefore, it is desirable for TEA practitioners to create flexible TEA models that generalise effectively to a wide range of opportunities and for these models to be independent of specialised software tools.

Surrogate models map inputs to outputs of more complex processes. Machine learning (ML) is often used to create these correlations and is increasingly being used for modelling, optimising, and monitoring thermal conversion processes [7]. However, surrogate modelling for SCWG has focused on predicting process outputs such as hydrogen or syngas yields [8–10]. Several studies have used these to suggest optimal processing parameters [8], screen catalysts [9], or create interpretable models to better understand the relationship between process parameters and biomass characteristics on gas yields [10]. Feedstock-specific surrogate models have also been developed to predict hydrogen yields for SCWG. For example, Shengagaraj et al. (2021) used an Artificial Neural Network (ANN) to predict the syngas yields from food waste biomass [11]. Similarly, Khan et al. (2023) created a model for the SCWG of sewage sludge, where they created a graphical user interface of their ML model. The model predicts the H$_2$ yield based on the proximate and ultimate analysis of the sample, as well as the input of gasification conditions [12]. In addition, Fózer et al. (2021) created an ANN surrogate model of

a microalgae SCWG reactor and used it within their economic and environmental analysis for methanol production [13].

In the broader context of hydrogen production and generation, ML has been widely applied to determine and develop efficient processes [14]. For example, Yahya et al. (2021) used an ANN coupled with a genetic algorithm and response surface methodology to optimise the production of hydrogen via steam reforming of toluene, finding the ANN to be a more robust predictor than response surface methodology [15]. Kargbo et al. (2023) utilised a bootstrapped aggregated neural network to represent waste wood gasification in their hydrogen production optimisation study [16]. Regarding predicting hydrogen production rates, Sultana et al. (2023) developed a Bayesian algorithm and Support Vector Regression (SVR) model to predict the hydrogen and methane yield via dark fermentation [17]. Model inputs included the pretreatment duration, feedstock concentration, and pH. Sezer et al. (2021) created an ANN model of an Aspen Plus simulation, representing a bubbling fluidised bed gasifier for hydrogen production [18]. The ANN was trained to predict the exergy value of the produced syngas based on the biomass' elemental composition, gasifier temperature, steam flowrate and fuel flowrate.

Outside of hydrogen production, ML surrogate models have been applied to a limited number of studies within TEA and Life Cycle Assessments (LCAs). Liao et al. (2020) developed a combined ML and kinetic-based process simulation to assess the Greenhouse Gas (GHG) emissions, energy, and product consumption of producing activated carbon from 73 different woody biomasses under different operating conditions [19]. Olafasakin et al. (2021) investigated replacing first principles modelling of pyrolysis kinetics with a Kriging-based reduced order model for predicting the pyrolysis yields of 314 feedstocks, where the model outputs were used within a biorefinery process model to predict the corresponding Minimum Selling Price (MSP) and GHG emissions [20]. Whilst Liao et al. (2020) and Olafasakin et al. (2021) both used ML to create surrogate process models for use within TEAs and LCAs, additional detailed process modelling was still required to use the surrogate model predictions. Therefore, the use of these models still requires user expertise, making such models ineffective for decision-making by most experimentalists and industrialists. In contrast, Huntington et al. (2023) presented an auto-ML approach for generating a process model surrogate of a fixed lignocellulosic bioethanol process flowsheet for use within a TEA, where the surrogate model mapped 21 key operating and cost parameters to the MSP [6]. Notably, these operating parameters allowed adjustment of the plant throughput, the feedstock composition, conversion efficiencies, and cost considerations. Their method used the Tree-Based Pipeline Optimisation Tool considering four ensemble regression models, Random Forests (RF), Stacking, Extra Trees, and Gradient Boosting. Their approach provided direct TEA outputs, negating the need for modelling expertise or further incorporation of the surrogate models within a broader modelling framework.

This study uses ML to create a surrogate model for the TEA of renewable hydrogen production from low-temperature SCWG (380–500 °C). The Gibbs reactor in Aspen HYSYS is used as the simulation basis. The carbon footprint of the proposed process is verified alongside the TEA results for the range of biomass feedstock compositions and processing capacities in three different geographic locations. The biomass' ultimate analysis, processing capacity, and geographic location for the facility are the surrogate model inputs and the model outputs are the nominal and 70% probability band for the Levelised Cost of hydrogen (LCOH). Three ML algorithms were investigated for the surrogate model: RF, SVR, and ANNs, as these algorithms have been previously investigated for predicting hydrogen production via SCWG [9,10]. Additionally, a reliability measure was developed to evaluate the confidence in the surrogate model's predictions for new biomass feedstocks inputted by a user. The novelty of this work lies in the creation of an ML surrogate model representing the TEA of hydrogen production via SCWG. Whilst surrogate models have been previously developed for SCWG for hydrogen production [8–13], this is the first study to create a surrogate model representing a TEA of the process. The best performing surrogate model has been made publicly available (doi.org/10.6084/m9.figshare.22811066). The purpose of the published model is to provide indicative production costs, enabling researchers and manufacturers to quickly determine the economic potential of feedstocks and facilitate comparisons with other hydrogen production technologies.

2. Methodology

A data-set of 40 biomass feedstocks was collected from experimental literature investigating low-temperature SCWG (380–500 °C). The ultimate analysis (carbon (C), hydrogen (H), oxygen (O) and nitrogen (N)) of each of these feedstocks was collated. A process simulation of the low-temperature SCWG and purification to renewable hydrogen was created for each of the biomass compositions in Aspen HYSYS. The simulation was based on a fixed SCWG temperature at 430 °C. This was selected owing to the economic benefit of low-temperature SCWG which reduces the energetic burden required to preheat the feedstock [1], and the recent experimental study into the SCWG of biomass wastewaters by Lee et al. (2023) which was conducted at this temperature [2]. A conservative residence time of 5 min was assumed, thereby providing sufficient residence time for the equilibrium as predicted by the Gibbs reactor to be attained. This was selected to exceed the residence times used experimentally for continuous low-temperature SCWG, where a 20s residence time achieved a total organic carbon reduction efficiency of 53.9–55.7% [2] and 88.4% at 150s [21]. A feedstock concentration corresponding to a Chemical Oxygen Demand (COD) of 75 g/L_{COD} was also selected.

Two hundred process simulations were created for the range of collected biomass compositions and five processing capacities (10, 20, 50, 100, and 200 m^3/h). These processing capacities were selected to allow for comparison to other low-carbon hydrogen technologies and represent realistic point source waste stream availability. A TEA and LCA was undertaken on each of the resulting simulations in three geographical locations (China, Brazil, and the UK) producing 600 data points. These geographic locations were selected as case studies with abundant wet wastes suitable for SCWG, i.e., Black liquor in China, vinasse in Brazil, and distillery
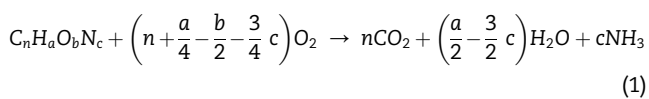
wastewater in the UK. These waste streams are also later used as case studies to compare the produced LCOH to alternative low carbon hydrogen production technologies. Furthermore, the selected three locations provide global coverage with differing economic inputs.

The TEA results are presented as the nominal LCOH ($/kg$_{H2}$) and the LCA results as the process' GHG emissions (kgCO$_2$eq/GJ$_{H2}$) for each combination of feedstock, processing capacity, and geographic location. A Monte Carlo simulation for each parameter combination was undertaken to illustrate the relative uncertainty around the nominal LCOH. The economic and environmental impact of transporting wastes to a larger capacity facility was also investigated. Finally, a ML surrogate model was created to predict the nominal, lower (5th), and upper (75th) LCOH computed from the TEA and Monte Carlo simulation using the feedstock's ultimate analysis, capacity, and geographic location as model inputs. Owing to the low utility usage of the SCWG process, the variability in GHG emissions between feedstocks was minimal. As such, the surrogate model was not trained to predict process emissions.

2.1. Data collection and pre-processing

The ultimate analysis consisting of the weight percent of C, H, O, and N was collected for each of the 40 biomass feedstocks and converted onto a 100% C, H, O, N basis. The compositions collected from literature are presented in the Supplementary Information, Table S1. Descriptive statistics of the data-set are presented in Table 1. The biomass feedstocks were selected to obtain a range of compositions to produce a generalisable surrogate model that can predict the LCOH for unseen, user inputted, biomass feedstocks.

The biomass' Ratio of Moles of Oxygen (RMO) to moles of oxidisable compounds (mol/mol) was calculated to determine the weight percent required for each feedstock to yield a COD of 75 g/L$_{COD}$. The RMO is the required amount of oxygen to fully oxidise a compound to CO$_2$, H$_2$O and NH$_3$ as expressed in Eq. 1. Eq. 2 defines the theoretical COD, where W (g/L) represents the solids concentration of oxidisable compound and Mr (g/mol) is the molecular mass of oxidisable compound.

$$C_nH_aO_bN_c + \left(n + \frac{a}{4} - \frac{b}{2} - \frac{3}{4}c\right)O_2 \rightarrow nCO_2 + \left(\frac{a}{2} - \frac{3}{2}c\right)H_2O + cNH_3 \quad (1)$$

$$COD = \frac{W}{Mr} * \left(n + \frac{a}{4} - \frac{b}{2} - \frac{3}{4}c\right) * 32 \quad (2)$$

The COD was used as the model basis as it is a required measurement of effluent streams and represents the stream's reduction potential, i.e. reducing power. Effluent streams with the same COD possess the same theoretical potential to produce H$_2$ regardless of composition, where more reduced compounds require a lower solids concentration than more oxidised compounds to attain the same COD. In contrast, the solids concentration also includes inorganic matter which does not contribute to the production of H$_2$. By using the COD as the model basis, the economic potential of the organic biomass content is easily interpreted.

Table 1 – Descriptive statistics of the biomass compositions collected from experimental literature for the SCWG of real biomass compounds.

Descriptive Statistic	Ultimate analysis (wt%)			
	C	H	N	O
Mean	47.82	6.11	1.98	32.39
Standard Deviation	17.69	3.06	1.77	17.05
Minimum Value	18.94	0.75	0.00	0.20
25th Percentile	38.01	4.43	0.70	16.97
50th Percentile	43.52	5.98	1.26	36.51
75th Percentile	57.39	6.65	3.19	46.83
Maximum Value	84.74	14.90	6.27	55.80

2.2. Process simulation

A temperature of 430 °C was used for the SCWG, owing to the economic benefit of low-temperature SCWG [1]. The COD for each biomass feedstock was fixed at 75 g/L$_{COD}$. For the considered biomass feedstocks, this translates to 5 wt% solids on average, though the actual content varies depending on the reduction potential of the biomass. This concentration was selected as low solids concentrations lead to increased hydrogen production through enhancing steam methane reforming and water gas shift reactions [1]. However, from an economic standpoint the solids concentration directly affects the energy balance, with more dilute feedstocks requiring greater energy to heat to supercritical conditions. The concentration was selected as a trade-off between these two factors. This consideration may require evaporation or dilution of the actual feedstock being evaluated but is not factored into the TEA or LCA as different dilution and evaporation requirements would vastly increase the model complexity. Costs and emissions associated with evaporation or dilution to the 75 g/L$_{COD}$ necessitates external quantification by the user.

A TEA was undertaken on the process simulation using five different processing capacities (10, 20, 50, 100, and 200 m^3/h). This led to 200 process simulations, considered over three geographical locations (China, Brazil, and the UK), resulting in 600 economic analyses. The TEA results were presented as the nominal LCOH.

The 50 and 100 m^3/h capacities yield between 7.5-10 and 15−20 MW of hydrogen, respectively. These results are directly comparable to green electrolysis LCOH prices produced by BEIS (10 MW) [22]. Furthermore, the range of capacities investigated represent realistic effluent production rates for the considered countries. For example, Brazil's Sebigas plant processing vinasse has a capacity of 500 tn$_{COD}$/day, corresponding to 277 m^3/h of wastewater at 75 g O$_2$/L COD concentration [23]. In addition, a 200 m^3/h throughput scale corresponds to a modest-sized pulp mill with a processing capacity of approximately 12,000 ADt/yr of pulp, based on 10 t $_{black\ liquor}$/t$_{ADt\ pulp}$ [24]. By comparison, China's largest pulp mill produces 1.2 million ADt/yr [25]. With regards to distillery wastewater, pot ale and wet draff are produced at rates of 7.9 L/L$_{alcohol}$ and 2.55 kg/L$_{alcohol}$ [26]. Using both these waste streams, the processing capacities explored in this study correspond to a distillery capacity between 5 and 104 million

litres/yr, noting that the largest operational Scottish Distillery is 100 million litres [27]. Considering anaerobic digestate as a feedstock, the 10 m^3/h throughput scale corresponds to approximately 500 kg/h of dry solids based on a 5 wt% solids concentration and digestate production at 0.87 kg/kg$_{feedstock}$ [28]. This is equivalent to an anaerobic digestion (AD) facility capacity of 100 kt/yr, where currently 20 facilities in the UK operate at a capacity >96 kt/yr$_{digestate}$.

2.2.1. Gasification

The SCWG reaction was modelled in Aspen HYSYS using a conversion reactor to decompose the unconventional biomass compound into its base compounds (H_2, O_2, N_2 and C). As such, only the ultimate analysis was required to represent each considered biomass compound. The stochiometric co-efficients for the decomposition reaction in the conversion reactor were modified for each biomass sample using a MATLAB script. This was followed by a Gibbs reactor to predict the gasifier effluent assuming full conversion to gaseous products and the attainment of equilibrium at the specified temperature and pressure. This is a common approach in techno-economic studies of SCWG [29]. For example, this method has been used previously for the valorisation of black liquor [4], digested sewage sludge [3], and soybean straw [5]. The simulation considers the achievement of thermodynamic equilibrium and complete biomass conversion to gaseous products. It is recognised that equilibrium may not be reached in industrial conditions and achieved gas yields may differ from those predicted by the Gibbs reactor. Also, formation of solid by-products, such as tar and char, may not be negligible. However, in the absence of extensive complete conversion data for low-temperature SCWG, the approach enables the evaluation of different feedstocks on an equivalent basis. As such, the results represent the economic potential for a biomass feedstock. Moreover, the continuous SCWG reactor is sized based on a relatively conservative residence time of 5 min, translating to an additional capital expense. This residence time was selected to exceed the reported experimental results for continuous low-temperature SCWG where a 20s residence time achieved a total organic carbon reduction efficiency of 53.9−55.7% [2] and 88.4% at 150s [21].

An additional reactor was used to convert 100% of the fuel bound nitrogen to NH_3, similarly to Ref. [3]. Most of the NH_3 is removed with the high-pressure water flash after the SCWG reactor and it is assumed no further separation is required. The formation of sulphur compounds and ash were not considered. In practicality sulphur would form H_2S during gasification which would be removed along with CO_2 during H_2 purification. The formation of ash would be removed with any char formed during gasification and be subsequently combusted.

To satisfy the simulation's energy balance, the heats of formation for the hypothetical biomass compounds were estimated by subtracting the heat of combustion of the free elements (carbon (−393.15 kJ/mol) and hydrogen (285.83 kJ/mol)) from the biomass' Higher Heating Value (HHV) [30]. A correlation was used to estimate the HHV for each biomass based on its elemental composition. The correlation created by Huang & Lo (2020) was used to estimate the feedstock's HHV given the correlation was established using a large number and range of biomass feedstocks [31].

2.2.2. Syngas upgrading

The Gibbs reactor model predicts a higher methane fraction in the product gas at temperatures around 400 °C compared to temperatures above 500 °C, as shown in Table S2 in the Supplementary Information. At lower temperatures, the formation of hydrogen through endothermic gasification reactions is inhibited, while the exothermic reactions that form methane are favoured [32,33]. The observed trend in increased methane fractions at lower temperatures therefore aligns with thermodynamic principles. Whilst the focus of this study is hydrogen production, higher reaction temperatures are heavily disadvantaged from an economic perspective owing to the higher energy burden required to heat the gasifier feed [1]. By shifting this methane fraction to hydrogen post-gasification using mature chemo-catalytic technology, the economic benefit of low-temperature SCWG can be exploited whilst still maximising hydrogen production.

To shift the reactor effluent towards hydrogen, the mature Steam Methane Reforming (SMR), High-Temperature Shift (HTS) and Low-Temperature Shift (LTS) technologies were employed. A fraction of the SCWG effluent was directed towards combustion to support the endothermic SMR reaction, ensuring the process remained energetically self-sufficient. The operating conditions and kinetics used to model the SMR, HTS and LTS reactors are presented in Table 2. The hydrogen produced was then recovered using a primary amine stripper employing monoethanolamine (MEA) as a mass separating agent to absorb the CO_2.

A process flow diagram of the evaluated hydrogen production process is presented in Fig. 1. After reducing the temperature of the SCWG effluent to sub-critical conditions and flash drum separation, a turbo-expander recovers the energy from the vapour as electricity. In addition, electricity is generated upon letting down the spent flue gas after it has been used for steam generation. Most of the generated electricity is utilised within the process. However, the unused fraction is exported for sale to the grid as renewable electricity.

2.2.3. Automation

The ActiveX function in MATLAB was used to automate the input of the different biomass compounds. The biomass properties were transferred from MS Excel to Aspen HYSYS via a MATLAB script. To ensure each feedstock was evaluated on the same basis, a set of constraints was defined to be adhered to by all simulations. Owing to the different feedstock compositions, each simulation required manual adjustments to achieve these same constraints.

- Split between combustion and SMR adjusted to maintain energetic self-sufficiency
- Steam to carbon ratio maintained at 5.5 mol/mol by adjusting water flowrate to SMR
- MEA flowrate adjusted to achieve hydrogen purity >99.5% v/v
- Temperatures adjusted to prevent temperature crosses in heat exchangers

2.2.4. Techno-economic analysis

The LCOH was computed for each biomass composition, processing capacity, and location combination. This was

Table 2 – Operating conditions and modelling parameters used in the process simulation.

Parameter	Value	Comments
SMR temperature (°C)	1000	Kinetics based on a commercial Ni/α-Al$_2$O$_3$ catalyst [34].
SMR pressure (kPa)	1000	
Steam/carbon ratio (mol/mol)	5.5	To avoid carbon formation on the catalyst.
HTS temperature (°C)	420	Power law kinetics) for a commercial iron-based catalyst [35].
LTS temperature (°C)	200	Power law kinetics for a commercial Sud-Chemie Cu/ZnO/Al$_2$O$_3$ catalyst [36].

calculated from the discounted cash flow analysis across the considered 25-year plant life. The costing models and investment analysis parameters as used in the authors' previous work were used for the TEA, summarised in Tables S3–4 in the Supplementary Information [24,37]. An 8% discount rate was used in line with Europe's hurdle rates for electricity generation costs from biomass sources, e.g. 8.3% for AD and 7.9% for dedicated biomass (5–100 MW) and energy from waste (combined heat and power) [38]. The economic models were created for three geographic locations (China, Brazil, and the UK). As such, different location factors, operator salaries, and renewable electricity prices were used between the techno-economic models. These are summarised in Table 3.

2.2.5. Feedstock cost

A universal method for computing the utility value of the feedstock was developed based on the HHV of the biomass relative to natural gas. Methane production from AD is an alternative treatment method for dilute biomass feedstocks. However, AD can only exploit the Biological Oxygen Demand of a feedstock, whereas SCWG exploits the COD. An efficiency factor of 70% was thus applied to the calculated HHV, reflecting a high Biological Oxygen Demand to COD ratio [44]. The feedstock's price was then computed based on the adjusted HHV relative to the HHV of natural gas and using the EIA's price projections [45].

2.2.6. Uncertainty analysis

An uncertainty analysis was undertaken on the LCOH for each biomass composition, processing capacity, and location considered. A Monte Carlo analysis was conducted comprising 2,000 simulations where the fixed capital (80%–150%), variable operating (80%–200%), feedstock cost (90%–130%), and renewable electricity prices (80%–200%) were stochastically varied using a uniform distribution of the outlined ranges. This produced a probability distribution of the LCOH for each parameter combination. The calculated 5th and 75th percentiles from the Monte Carlo simulations were predicted along with the nominal LCOH by the surrogate model. This provided the 70% probability band of the LCOH for the investigated feedstock, capacity, and geographic location.

2.3. Life cycle assessment model

A cradle-to-gate LCA was undertaken for each biomass feedstock for the two products, hydrogen and renewable electricity. The considered functional units were 1 GJ of hydrogen (GJ$_{H2}$) and 1 MWh of renewable electricity. The emissions were allocated between these two products using energy allocation.

As the model was created for waste biomass feedstocks, no feedstock emissions were allocated. Furthermore, the CO$_2$ emitted is of biogenic origin and so does not contribute to the overall GHG emissions. Carbon capture units were not considered owing to the uncertainty around storage arrangements for small production streams, such as those generated in this study. The products were compared to other hydrogen production methods and each country's respective electricity grid emissions. The GHG emissions for MEA and water were obtained from the ecoinvent 3.7 inventory [46]. Emissions for transportation were considered using EURO 6 freight lorries of
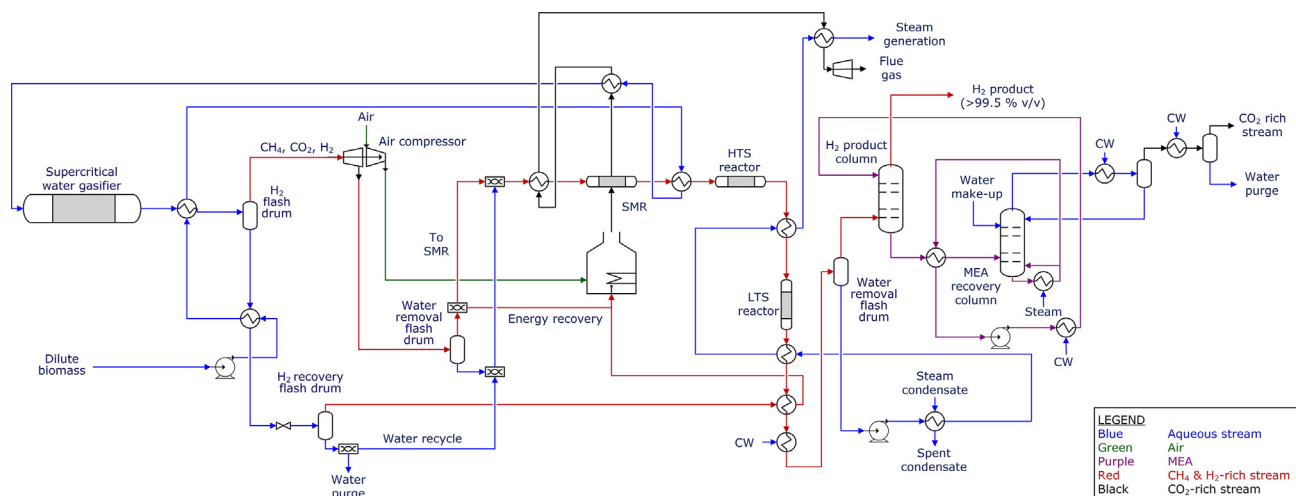

Fig. 1 – Process flow diagram of the low-temperature SCWG of biomass feedstocks for renewable hydrogen production.

Geographic Location	Location Factor	Average Operator Salary (yr) [39]	Renewable electricity price (kWh)	Currency conversion [43]
China	0.66	¥ 172,172 ($ 24,104)	¥ 0.75 ($ 0.105) [40]	0.14
Brazil	1.06	R$ 81,840 ($ 15,550)	R$ 0.315 ($ 0.059) [41]	0.19
UK	1.04	£ 33,776 ($ 41,207)	£ 0.126 ($ 0.154) [42]	1.22

Table 3 − Location factors, operator salaries, and renewable electricity selling price for the different global locations considered for the TEA. For comparison, the values are converted to 2022 US$ and presented in brackets.

16−32 tn capacity. A full life cycle inventory can be found in Table S5 in the Supplementary Information. Whilst cooling and process water were assigned emissions, the emissions associated with dilution or evaporation of feedstocks to the 75 g/L$_{COD}$ were not considered.

2.4. Transportation

In the TEA and LCA, each feedstock was assessed at its point of origin, meaning no transportation costs or emissions were included. However, as the impact of capacity on processing costs is assessed, an investigation into of the impact of transporting localised waste streams to larger facilities is warranted. This analysis was undertaken on distillery wastewater in the context of the UK. The cost of transporting the feedstocks was taken as £ 0.25 t/km based on costs for digestate transportation [47] and updated using the ratio of UK diesel prices in 2022 to 2016. The waste transportation capacity was selected based on the evaluated facility sizes (10, 20, 50, 100 and 200 m^3/h). Thereby, a 100 m^3/h facility could be located at a facility producing a waste stream of either 100, 50, 20, or 10 m^3/h, necessitating the additional waste to achieve the 100 m^3/h capacity to be transported to it. A nominal 30 km transport distance was selected.

2.5. Surrogate model

For each feedstock, six input variables were provided to each model, including the weight percentage of C, H, O, and N (descriptive statistics of the biomass compositions are presented in Table 1), processing capacity (10, 20, 50, 100 or 200 m^3/h), and geographic location (China, Brazil, or the UK). The geographic location was defined as 1 (China), 2 (Brazil), or 3 (the UK) to input into the model. The outputs of the model were the nominal LCOH and corresponding 5th and 75th percentiles, representing the 70% probability band. Due to minimal variability in the process emissions across different feedstocks and capacities, the surrogate model was not trained to predict the process emissions. Three ML algorithms, RF, SVR, and ANNs, were investigated for the surrogate model, as they have been previously considered for predicting hydrogen production via SCWG [9,10].

2.5.1. Model optimisation and evaluation

The 600 TEA combinations were split into training, validation, and test sets. As the hydrogen yield varied between biomass feedstocks, the feedstocks were distributed among these sets. Thereby, if a biomass feedstock was placed in the test set, the entire set of parameter combinations for that feedstock, i.e. processing capacities and geographic location, was also included in the test set. This approach ensured that

the model was trained to generalise across feedstock compositions rather than capacity and location and supports the goal of developing a generalisable model to evaluate the economic potential of hydrogen production from different biomass feedstocks. The data-set was split into a training set of 360, a validation set of 120, and a test set of 120 parameter combinations. Distributing the biomass feedstocks among the sets resulted in 24 biomass feedstocks in the training set, 8 in the validation set, and 8 in the test set. The best-performing hyperparameters were selected based on cross-validation performance, ensuring that the test set's performance indicated the model's generalisation potential for user input feedstocks. To optimise each ML algorithm a 4-fold cross-validation procedure was undertaken on the combined training and validation sets using an exhaustive grid search. The hyperparameters that were optimised for each algorithm are presented in Table 4. GridSearchCV from scikit-learn was used to determine optimal hyperparameters for each ML algorithm [48]. During the cross-validation process, the Root Mean Squared Error (RMSE) was used as the performance metric for each algorithm and as the loss function in the ANN.

An ensemble of predictions is produced by the RF algorithm, with the final output being the average of each decision tree's prediction. Ensemble methods typically have higher prediction accuracy because they reduce dispersion error and bias by averaging model predictions. They have previously shown improved prediction performance for hydrogen production via SCWG [10]. Consequently, an ensemble approach was also applied to ANNs, which randomly initialise starting weights and biases. This diversity allows each model to capture different aspects of the data. The average prediction from ten ANN models using the optimised hyperparameters was used to evaluate the algorithm's performance. Unlike ANNs, SVR does not contain random elements during model training, so an ensemble of SVR using optimised hyperparameters was not implemented.

After determining the optimal hyperparameters for each algorithm, it was evaluated on the test set to provide an indicative performance measure of the model's generalisability to unseen feedstocks. Three performance metrics were used to assess the model's prediction accuracy: RMSE, Mean Absolute Percentage Error (MAPE), and the determination coefficient (R^2). Each metric has different advantages: RMSE measures the standard deviation of the prediction errors, penalising large errors and making it more sensitive to outliers; MAPE measures the absolute error between the true and predicted values and presents them as a percentage, being less sensitive to larger errors than RMSE; and R^2 represents the fitness of the model to the true values and provides an intuitive result, with a value of 1 representing a perfect fit.

Table 4 – Hyperparameters and ranges considered for each algorithm during the cross-validation grid search procedure.

Random forests	Support vector regression	Artificial neural network
Number of trees (10–500)	L2 Regularisation penalty (1.1–1000)	Number of layers (1–3)
Maximum number of features for split (1–6)	Kernel type (linear, polynomial, radial basis function, sigmoidal)	Neurons in each layer (2–256)
Maximum depth of the tree (10–500)	Kernel coefficient (0.01–100)	L2 Regularisation penalty (0.00001–0.1)
Minimum number of samples before split (1–10)	Degree (for polynomial kernel function only) (1–3)	Learning rate (0.00001–0.1)
Minimum data in a leaf (1–10)	Epsilon (0.001–10)	Epochs (1000–10,000)
Bootstrap sampling (with or without replacement)		Batch size (2–256)

Eqs (3)–(5) present these metrics, where N is the number of datums, y_j is the true value, $\hat{y}_t$ is the predicted value, and y_M is the mean value. The published surrogate model was trained on the entire data-set using the algorithm and hyper-parameter set that produced the most accurate predictions during the cross-validation procedure.

$$RMSE = \sqrt{\frac{1}{N} \sum_{t=1}^{N} \left(y_j - \hat{y}_t \right)^2} \tag{3}$$

$$MAPE = \frac{1}{N} \sum_{t=1}^{N} \frac{y_j - \hat{y}_t}{y_j} \tag{4}$$

$$R^2 = \frac{\sum_{t=1}^{N} \left(y_j - y_M \right)^2}{\sum_{t=1}^{N} \left(\hat{y}_t - y_M \right)^2} \tag{5}$$

2.5.2. Feature importance

ML models are often referred to as "black box" models due to the complexity of their internal workings, which are not easily interpretable. To address this interpretability challenge, feature importance methods are employed. One such method is SHapley Additive exPlanation (SHAP) values. These values assign a contribution score to each feature, indicating its importance in the model's output. By utilising SHAP values, users can gain a better understanding of the relationships between input features and model outputs [49]. In previous studies, SHAP values have been applied to identify redundant input data, thereby reducing the computational cost of ML models [9]. However, in this work, SHAP values are used to highlight the relative importance of the input features. The SHAP values were obtained for the best-performing ML model using the SHAP library in Python.

3. Results and discussion

The TEA and LCA results are presented for the 600 parameter combinations (biomass composition, capacity, and geographic location). The impact of feedstock transportation is also presented and discussed. The production costs and process emissions are compared to both MW-scale electrolysis using renewable electricity and SMR with CCS (Carbon Capture and Storage). The performance of the three ML algorithms is also presented and compared.

3.1. Techno-economic analysis

The LCOH for the 600 techno-economic parameter combinations were computed, achieving levelised costs of 1.66–11.89 $/kg$_{H2}$ (China), 2.61–16.82 $/kg$_{H2}$ (Brazil), and 2.46–18.73 $/kg$_{H2}$ (UK). Different feedstock compositions and capacities led to significant variations in the economic outcome.

3.1.1. Location

Fig. 2 presents the LCOH for the 600 techno-economic parameter combinations. Fig. 2a presents the results for China, 2b for Brazil, and 2c for the UK. The geographic location produces a considerable difference in the LCOH. The UK produced the highest prices, followed by Brazil and then China. The higher prices for both the UK and Brazil are attributed to higher capital and operating costs (Table 3).

3.1.2. Processing capacity

The capacity of the SCWG facility is shown to have a substantial impact on the LCOH (Fig. 2a–c). As the scale increases, the LCOH decreases following an inverse power law relationship. The observed power law relationship is likely because most equipment cost correlations follow power law relationships. Furthermore, in capital cost estimation the 'six-tenths rule' can be applied to update the capital cost of a plant or processing equipment based on the cost of the same item at a different capacity by using a 0.6 exponent (average for the chemical industry) [50]. Applying a power law to the average LCOH for each geographic location gives rise to three different correlations, each with an $R^2 > 0.93$ and exponents ranging between −0.48 and −0.58. However, these correlations represent the average LCOH and the correlation for each biomass composition and corresponding location would be different (Fig. 2a–c). This prevents the use of a simple correlation to predict the LCOH for different feedstocks and illustrates the utility of a TEA surrogate model applicable to a wide range of inputs.

3.1.3. Uncertainty analysis

A Monte Carlo simulation comprising 2,000 simulations was undertaken on each of the 600 techno-economic scenarios by varying the fixed capital, variable operating, feedstock, and renewable electricity costs within the uncertainty ranges summarised in Section 2.2.6 Uncertainty Analysis. All parameters were varied stochastically using a uniform distribution between the defined ranges. The LCOH for each stochastic parameter combination was computed and the 5th,
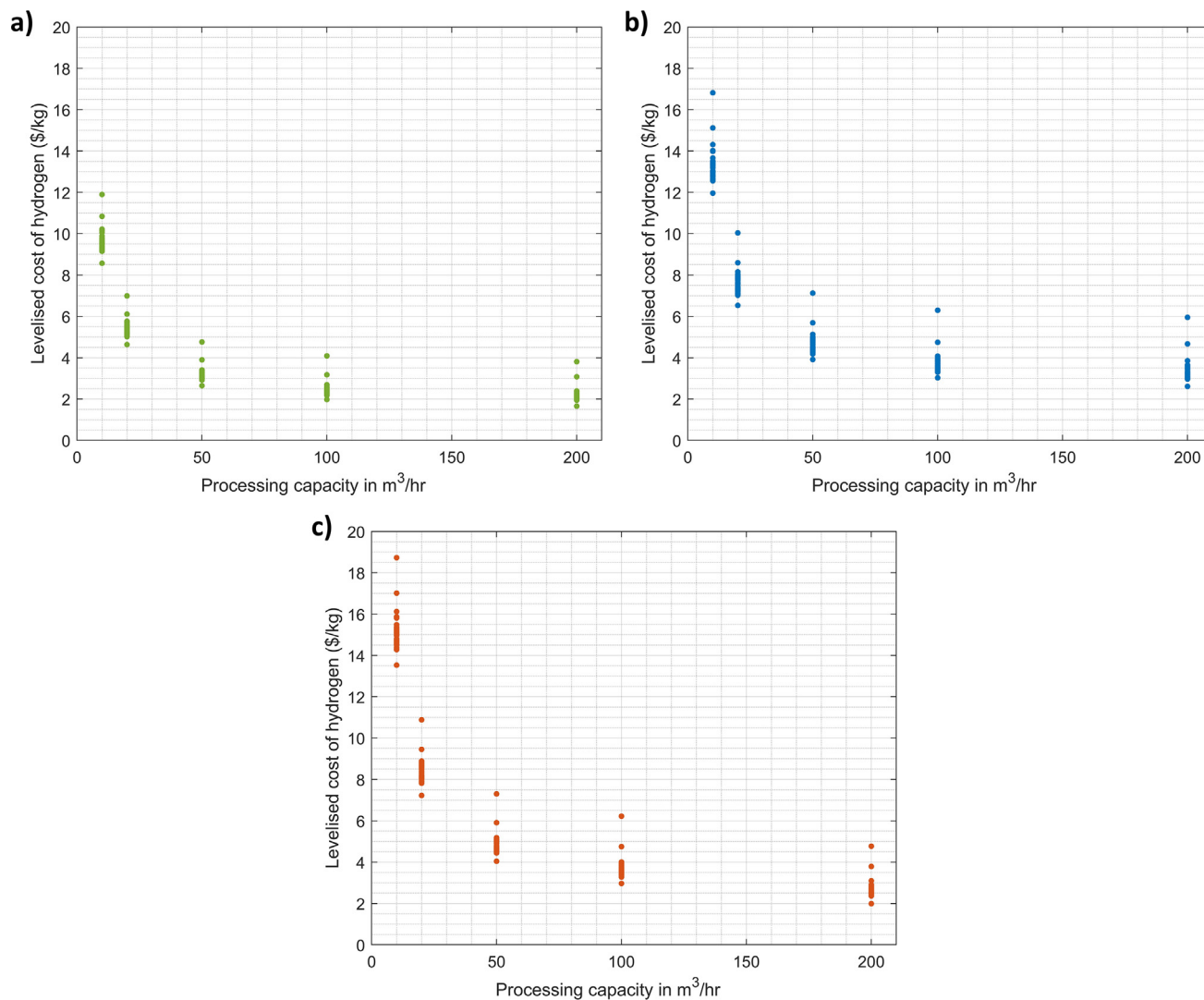
Fig. 2 − a−c: LCOH ($/kg$_{H2}$) for different processing capacities (m^3/hr). a) Presents the results for China, b) presents the results for Brazil, and c) presents the results for the UK. Each location has 40 data points representing the biomass feedstocks and is presented using the same y-axis.

25th 50th, 75th, and 95th percentiles were calculated. The 5th and 75th percentiles represent the 70% probability band for the LCOH. On average, this probability band displayed a −13% and +28% deviation from the nominal value for all parameter combinations. The deviations were similar for all cases, ranging from −22% to +32%. The greater positive variability observed is attributed to the larger upward deviations assigned to the uncertainty parameters.

3.1.4. Gate fee

Some feedstocks could command a gate fee to handle their disposal, forming an additional source of revenue. For example, the median gate fees in the UK for AD and energy from waste disposal options are £30/t and £95/t, respectively [51]. Food waste is a typical AD feedstock [47] and is used here to illustrate the impact of including a gate fee for SCWG in the UK. Gate fees of £10/t, £20/t, and £30/t ($12/t, $24/t, and $37/t), up to and equalling that of AD, were selected (Fig. 3). Notably, the inclusion of a gate fee significantly reduces the LCOH, creating

economically viable solutions at smaller capacities. At a capacity of 10 m^3/h, a gate fee of $37/t (equalling that of AD) leads to an LCOH of $4.82/kg, comparable to MW-scale electrolysis using renewable electricity, which ranges from $4.81/kg to $6.31/kg [22]. However, at a capacity of 20 m^3/h, a gate fee of only $12/t is required to achieve a comparable LCOH, and a gate fee of $37/t results in a negative LCOH. At capacities >50 m^3/h, the addition of a gate fee results in a low or even negative LCOH (Fig. 3), demonstrating the technology's potential to outperform AD as a waste treatment option and the economic potential of valorising waste streams at these capacities.

3.2. Life cycle assessment

The range in cradle-to-gate GHG emissions of the evaluated feedstocks in Brazil and China was 0.32−0.65 kgCO$_2$eq/GJ$_{H2}$ (0.038−0.078 kgCO$_2$eq/kg$_{H2}$) with an average of 0.46 kgCO$_2$eq/GJ$_{H2}$ (0.055 kgCO$_2$eq/kg$_{H2}$). In the UK, the GHG emissions ranged between 0.25 and 0.52 kgCO$_2$eq/GJ$_{H2}$ (0.031 and 0.063
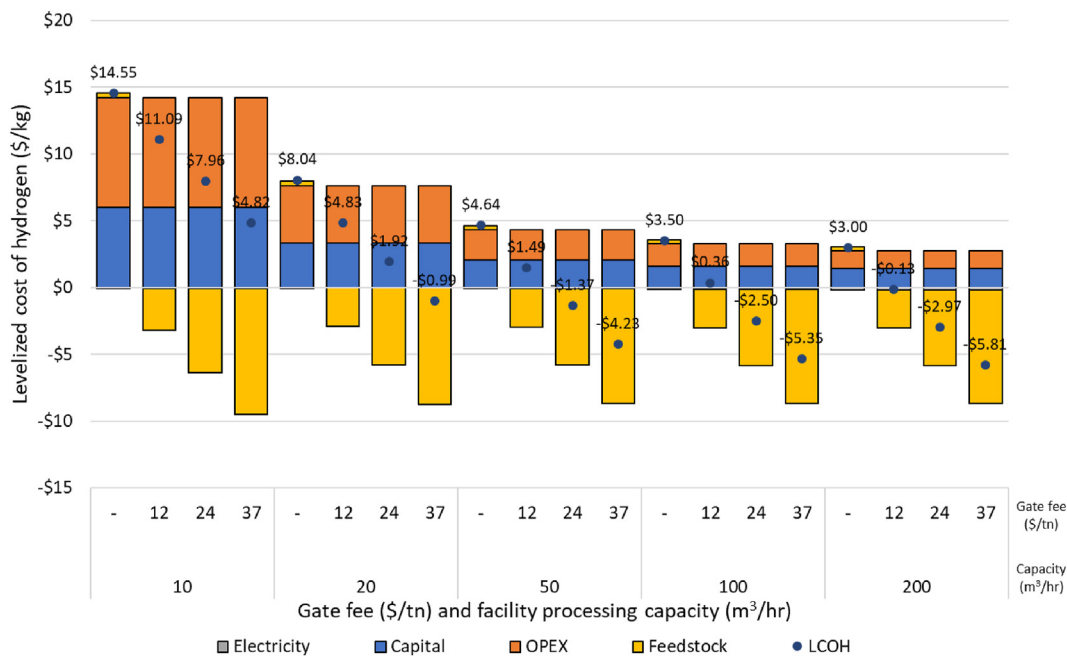
Fig. 3 – Impact of the inclusion of a $12/t, $24/t and $37/t gate fee on the LCOH for food waste biomass.

$kgCO_2eq/kg_{H2}$) with an average of 0.37 $kgCO_2eq/GJ_{H2}$ (0.044 $kgCO_2eq/kg_{H2}$). The difference between countries is due to the use of global emission factors for both Brazil and China and European emission factors for the UK. The low overall emissions are attributed to its energetic self-sufficiency of the SCWG process, negating the need for external energy sources. The only utilities used throughout the process are MEA make-up to account for losses during CO_2 removal and deionised water for both cooling and water make-up in the stripper. The GHG emission ranges for all feedstocks considered comfortably meet the European Union CertifHy scheme for low carbon hydrogen (≤ 36.4 $kgCO_2eq/GJ_{H2}$) based on a 60% reduction in emissions from SMR [52]. In contrast, SMR with CCS produces 8 $kgCO_2eq/GJ_{H2}$, at 90% capture efficiency [53]. However, including emissions associated with natural gas leakage increases this estimate to 21 $kgCO_2eq/GJ_{H2}$ [53], over an order of magnitude higher than estimates for SCWG.

The emissions attributed to the exported renewable electricity were also minimal, with an average of 0.04 $kgCO_2eq/$ MWh for Brazil and China and 0.03 $kgCO_2eq/MWh$ for the UK. This is in comparison to the grid intensity of China, Brazil, and the UK being 850 $kgCO_2eq/MWh$ [54], 292 $kgCO_2eq/MWh$ [54], and 194 $kgCO_2eq/MWh$ [55], respectively.

3.3. Transportation impact

The impact of transporting wastes to a larger facility was investigated for both the economics and process emissions and is presented in Fig. 4a and b for distillery wastewater in the UK. Due to the dilute nature of pot ale, only draff (solids content 21.6 wt% [26]) was considered for transportation in this analysis.

Transporting draff to a different distillery for processing demonstrates a decrease in the LCOH compared to solely processing point source distillery waste (Fig. 4a). For example, a distillery producing 10 m^3/h of wastewater at 75g/ L_{COD} yields a LCOH of $15.37/kg by processing only point source waste. However, transporting enough draff to operate a SCWG facility of 50 m^3/h (located at the same distillery producing 10 m^3/h) leads to a decrease in the LCOH to $8.26/ kg. This decreasing trend in LCOH is demonstrated for all point source feedstock processing capacities between 10 and 50 m^3/h. The observed decrease is due to the capital and operating cost intensity decreasing more appreciably than the added cost of transportation. Conversely, at a point source of 100 m^3/h of wastewater, the transportation of draff to support a 200 m^3/h SCWG plant increases the LCOH from $3.51/kg to $3.78/kg.

Regarding process emissions (Fig. 4b), any transportation of waste proves detrimental to the GHG emissions. In all cases considering draff transportation the transport emissions dominate the overall process emissions. However, the emissions are still well below SMR with CCS, which are 8 $kgCO_2eq/GJ_{H2}$ (excluding emissions associated with natural gas leakage) [53].

It is important to note that the transportation of biomass is logistically challenging. Studies considering large capacity plants often explore decentralised supplies that enable satellite pre-processing or combine multiple modes of transportation, depending on the transportation distance [56]. The assumptions made for this analysis do not consider these complexities, and further investigation should be undertaken for specific feedstocks, alongside the actual transport distances required. In addition, biomass compositions may be more or less dilute than considered here. This would change the associated transport costs, as evaporation would occur at the point of origin, and dilution would occur at the point of processing.
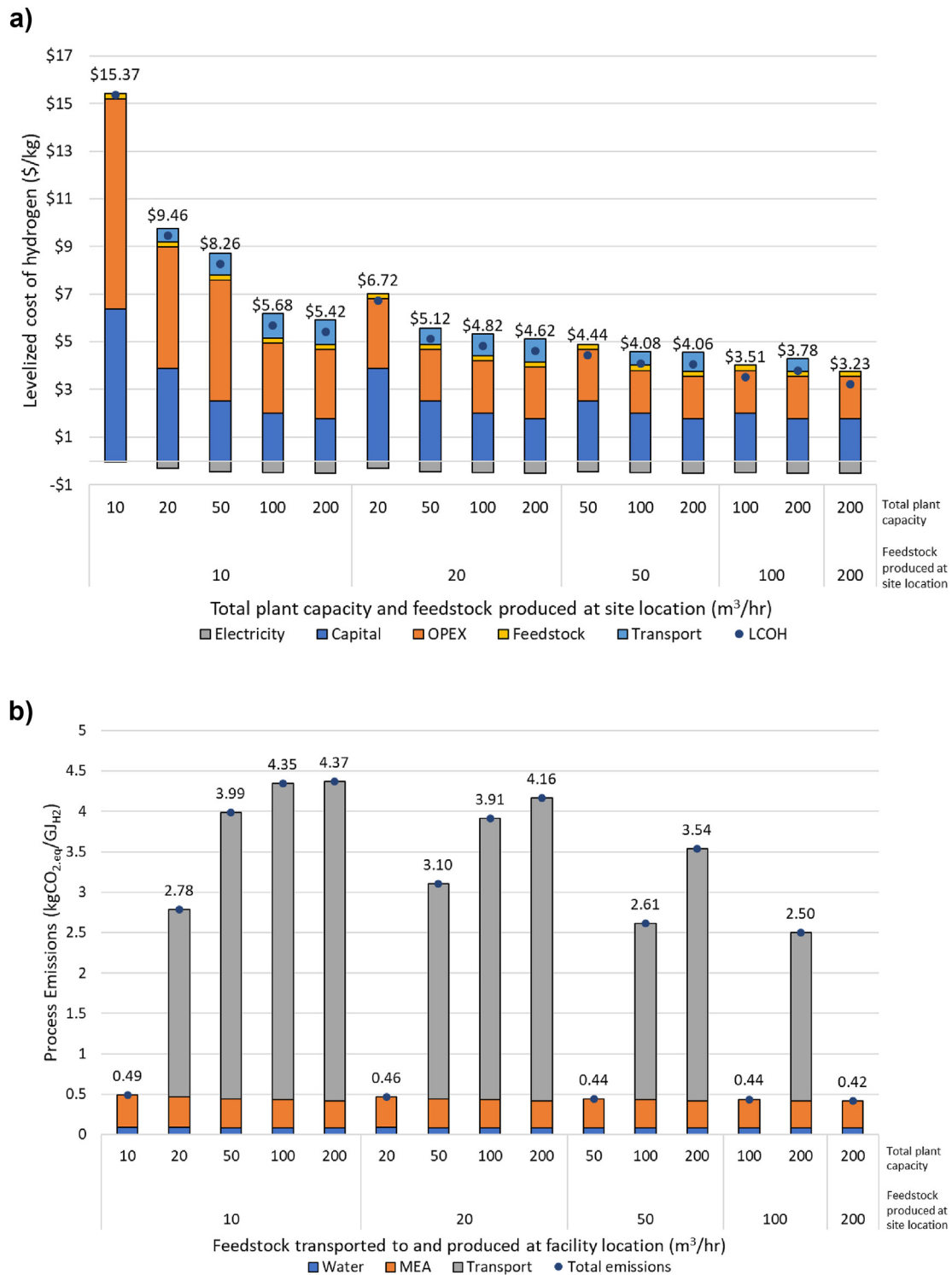
Fig. 4 — a—b: Impact of transporting distributed waste streams to larger processing facilities on the LCOH ($/kg$_{H2}$) (4a) and process emissions (kgCO2eq/GJ$_{H2}$). (4b). Analysis results are for distillery wastewater in the UK.

3.4. Comparison to alternative low carbon hydrogen production

Hydrogen production costs are significantly impacted by capital costs, technology efficiency, capacity factors, energy costs, and the plant location [57]. Fig. 5 presents the 70% probability band of the LCOH at the considered SCWG capacities for black liquor in China, vinasse in Brazil, and distillery wastewater in the UK. These biomass feedstocks were selected as they represent feedstocks readily available in
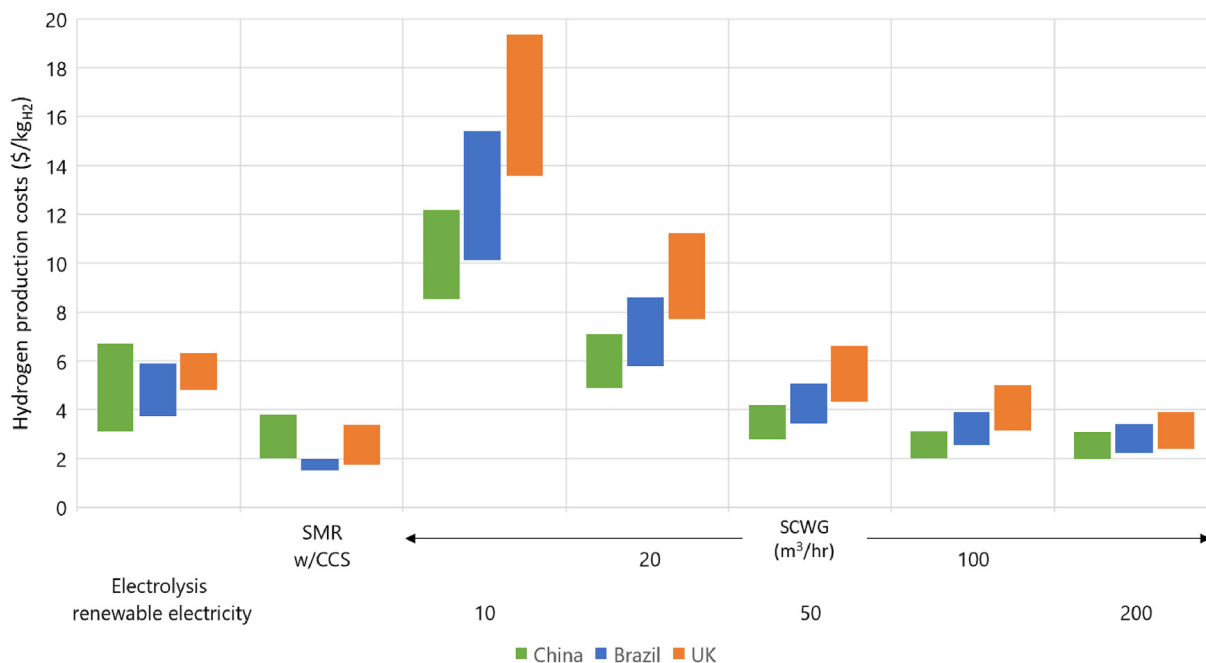
Fig. 5 – Comparative LCOH for MW-scale electrolysis using renewable electricity, SMR with CCS, and SCWG for black liquor in China, vinasse in Brazil, and distillery wastewater in the UK. The displayed results exclude transportation or gate fee considerations.

these countries. The resulting LCOH's are compared to each country's cost estimates for alternative low carbon hydrogen production methods, namely, hydrogen production via MW-scale electrolysis using renewable electricity and SMR with CCS. Estimates are obtained from the IEA for China [58,59] and Brazil [60], and BEIS for the UK [22].

In all countries, at a SCWG capacity of 50 m^3/h, the LCOH (2.76–4.21 $/$kg_{H2}$ for China, 3.41–5.07 $/$kg_{H2}$ for Brazil, 4.31–6.62 $/$kg_{H2}$ for the UK) is cost competitive with hydrogen production via MW-scale electrolysis using renewable electricity (3.10–6.70 $/$kg_{H2}$ for China, 3.70–5.90 $/$kg_{H2}$ for Brazil, and 4.81–6.31 $/$kg_{H2}$ for the UK). This demonstrates the potential for isolated feedstock valorisation using low-temperature SCWG at capacities >50 m^3/h. Additionally, in China SCWG capacities >50 m^3/h are comparable to SMR with CCS (2.00–3.80 $/$kg_{H2}$) and in the UK, the 200 m^3/h SCWG capacity achieves a similar LCOH (2.36–3.92 $/$kg_{H2}$) to SMR with CCS (1.74–3.40 $/$kg_{H2}$). However, SMR with CCS is notably cheaper than even the largest SCWG facility size in Brazil. As SMR is the dominant commercial hydrogen production technology globally, the lower production costs for SMR with CCS are unsurprising.

Importantly, SCWG is ideally suited to wet feedstocks that are uneconomical for use via conventional energy recovery methods. Therefore, valorising these feedstocks via SCWG has limited resource competition and represents a renewable hydrogen source from otherwise under-utilised resources. In contrast, MW-scale electrolysis and SMR utilise renewable electricity and natural gas, both of which have numerous alternate uses and competition. As such, electrolysis and SMR are subject to price fluctuations in world energy markets. This means that changes in global energy markets directly affect the predicted prices in Fig. 5. A timely example is natural gas

prices, which averaged $6.45/MMBTU in 2022, up from $2.03/MMBTU in 2020 [61].

3.5. Surrogate model

The optimal hyperparameters obtained during the 4-fold cross validation procedure are presented in Table 5. Table 6 illustrates the performance metrics for the ML models using the optimal hyperparameters for the nominal LCOH on both the validation and training sets. Overall, ANN's achieved the highest model performance for both the validation and test sets, achieving accuracy values of MAPE: <4.6%, RMSE: <0.39, and R2: >0.99 on the test set. This is likely due to their ability to combine inputs into new features and thus utilise the relationship between inputs. A parity plot of the ANN's performance on the test set is presented in Fig. S1 in the Supplementary Information. Owing to the comparison of models, optimisation of hyperparameters, exhaustive grid search, and 4-fold cross validation procedure the outcome reflects the final accuracy of the ML task. Since the hyperparameters have been selected based on the validation set and the training, validation, and test sets were segregated based on biomass composition, the models' performance on the test set is a robust indicator of generalisation to new, unseen, biomass feedstocks. This is important as it represents the model's accuracy when utilised by researchers assessing their feedstock compositions.

The relative feature importance for the ensemble of ten ANN models is presented using SHAP values in Fig. 6. Fig. 6a presents the absolute significance of each feature, larger values indicate a greater impact on the model output (LCOH). Regarding the relative importance, the processing capacity was the dominant feature for the ML models. This is

Table 5 — Optimal hyperparameters determined during the 4-fold cross-validation grid search.

Random forests	Support vector regression	Artificial neural network
Number of trees: 100	L2 Regularisation penalty: 100	Number of layers: 1
Maximum number of features for the split: 2	Kernel type: radial basis function+	Neurons in each layer: 64
Maximum depth of the tree: 100	Kernel coefficient: 4	L2 Regularisation penalty: 0.001
Minimum number of samples before split: 2	Degree (for polynomial kernel function only): N/A	Learning rate: 0.001
Minimum data in a leaf:1	Epsilon: 0.5	Epochs: 5000
Bootstrap sampling: without replacement		Batch size: 16

unsurprising considering the substantial variability in LCOH observed across different capacities, as shown in Fig. 2. Geographic location was the second most important feature, attributed to the different economic inputs (Table 3) producing different LCOH's for the same biomass composition and processing capacity combinations. Among the biomass composition features, the hydrogen content demonstrated the greatest impact. Fig. 6b displays the impact of each feature using a bee swarm plot, where negative values indicate a negative impact on the model output (LCOH). The feature value scale from pink (high) to blue (low) indicates the feature input value. For example, a high processing capacity (coloured in pink), has a negative impact on the model output, thereby reducing the LCOH. It is also evident that higher H wt% leads to a reduction in the LCOH. This is to be expected as biomass with a higher hydrogen content yields more hydrogen, thereby lowering the LCOH. Increases in the other composition features all had a positive impact on the model output, indicating that higher C, N, and O wt% leads to an increase in the LCOH. This can be attributed to a greater wt % of these elements reducing the H wt%, subsequently decreasing the hydrogen yield obtained from the biomass.

The published model uses an ensemble of ten ANNs trained using the entire data-set of 600 TEAs using the optimal hyperparameters determined during the cross-validation procedure. The model inputs are the biomass' ultimate analysis, the processing capacity, and the geographic location. The nominal, lower (5th), and upper (75th) LCOH are

the model outputs. The surrogate model was trained using data from five specific processing capacities (10, 20, 50, 100, and 200 m^3/h). However, the model is intended to predict the LCOH for the range of capacities 10−200 m^3/h. To demonstrate the model's ability to interpolate between the capacities used for training, Table S6 in the Supplementary Information presents a comparison between the model predictions with simulated results for an unseen biomass sample in Brazil. Processing capacities of 10, 15, 20, 35, 50, 75, 100, 150 and 200 m^3/h were considered for the comparison. All the model predictions achieved a percentage error less than the MAPE of 4.42% obtained over the test set when compared to the simulated results. This low percentage difference highlights the model's capability to accurately predict beyond the specific training capacities used during its development, thus demonstrating its predictive ability. Extrapolation beyond the scales considered during model development (10−200 m^3/h) is not permitted by the model and is therefore not demonstrated.

3.5.1. Model uncertainty

The accuracy of a ML model's prediction on new, unseen inputs depends on this data's similarity to the model's training data. A method to estimate model uncertainty can be used to determine when this new data deviates significantly from the training set. This can be used to estimate when the models produce unreliable predictions. This is important for predictions made using new biomass samples inputted by the

Table 6 — Performance metrics for the ML algorithms. Metrics are displayed for both the validation and testing sets. The best performing model for each metric is presented in bold.

| Prediction	Data-set	Evaluation metric	RF	SVR	ANN
Nominal	Validation	RMSE	0.414	1.321	**0.197**
		MAPE	3.39%	19.7%	**1.56%**
		R^2	0.989	0.885	**0.998**
	Testing	RMSE	0.303	1.898	**0.291**
		MAPE	**4.00%**	39.3%	4.42%
		R^2	0.994	0.761	**0.994**
5th percentile	Validation	RMSE	0.332	1.170	**0.166**
		MAPE	3.16%	20.5%	**1.47%**
		R^2	0.990	0.881	**0.998**
	Testing	RMSE	**0.264**	1.758	0.279
		MAPE	**0.041**	0.425	4.58%
		R^2	**0.994**	0.731	0.993
75th percentile	Validation	RMSE	0.532	1.664	**0.236**
		MAPE	3.45%	17.6%	**1.63%**
		R^2	0.988	0.885	**0.998**
	Testing	RMSE	0.394	2.313	**0.389**
		MAPE	**4.07%**	35.4%	4.43%
		R^2	0.994	0.777	**0.994**

a)

b)
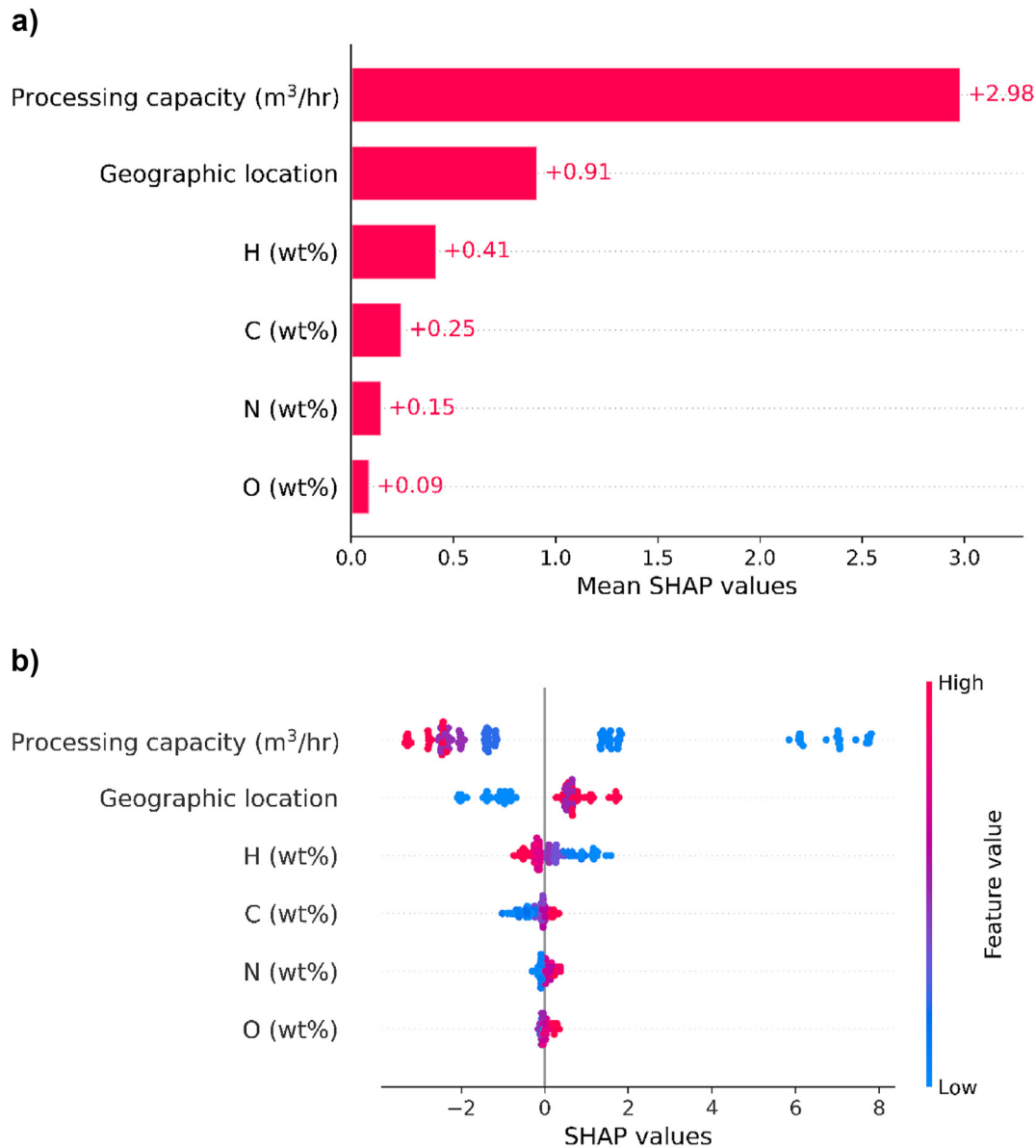
Fig. 6 – a–b: Feature importance of the model inputs on the LCOH Predictions using SHAP values. a) Absolute importance of input features on model output. b) Impact of input features on the model output. High feature values (inputs) are displayed in pink and low feature values are displayed in blue.

end user. In the ensemble approach, each ANN has different weights and biases owing to random initialisation. The diversity between each model will be greater in regions that were less well represented in the training data. Therefore, greater variance between the model predictions is observed in these regions. As such, the variance between the ensemble of predictions gives an indication of the model's uncertainty, with larger variations between predictions suggesting greater model uncertainty [62]. By setting a threshold for the allowable variance between predictions, unreliable predictions can be identified. This approach is similar to anomaly detection using autoencoders where an anomaly threshold is set by a reconstruction error [63].

For the published model, the permissible uncertainty threshold was set as the maximum variance observed for the nominal predictions during a 5-fold validation procedure on the entire data-set (600 parameter combinations). I.e. the ensemble models were trained on 80% of the data and 20% of the data was held back from training (the validation set). This was repeated five times for different folds in the data. The maximum variance observed on the validation sets was used as the uncertainty threshold. As an additional indication of uncertainty, it is known that the lower, nominal, and upper LCOH should be predicted in ascending order. In instances where this is not upheld, the model inputs represent an area poorly represented during model development.

To illustrate this principle, Table 7 presents the model predictions for three fictitious biomass compositions at different capacities and locations. The predictions are classified as anomalous if the prediction variance exceeds the

Table 7 – Surrogate model predictions for fictitious biomass compositions at different processing scales and geographic locations. The predictions are classified as anomalous if the prediction variance exceeds the variance threshold, and implausible if the predicted lower, nominal, and upper LCOH are not in ascending order.

Fictitious biomass composition				Scale (m³/hr)	Location	LCOH ($/kg_{H2})			Anomalous prediction	Implausible prediction
C	H	N	O			Lower	Nominal	Upper		
35	15	15	35	15	China	6.85	8.19	9.12	✓	✗
				35		3.57	4.16	3.18	✓	✓
				150		2.46	2.54	2.02	✓	✓
40	15	5	40	5	Brazil	12.71	14.3	18.14	✗	✗
				150		2.33	2.37	3.52	✗	✗
				250		2.43	2.17	3.1	✗	✓
40	21	0	39	20	UK	6.06	6.23	8.35	✗	✗
				80		2.24	2.09	2.67	✓	✓
				110		1.81	1.63	2.62	✓	✓

uncertainty threshold, and implausible if the lower, nominal, and upper LCOH are not predicted in ascending order. All predictions for the first composition trialled were deemed anomalous. This is attributed to the unrealistic biomass composition, as the high nitrogen and hydrogen content is unlike the compositions used for training. Despite this, in two out of three instances the model produced plausible predictions, i.e. the lower, nominal, and upper predictions were in ascending order. Contrastingly, for the second biomass composition, all predictions were below the uncertainty threshold and not deemed anomalous. This composition was representative of a realistic biomass composition, and therefore likely represented by the training set. However, at a scale of 250 m³/h the model prediction was implausible but was not detected as an anomaly. This capacity exceeded the range used during model training (10–200 m³/h). Therefore, the implausible prediction is attributed to model extrapolation beyond the region used during training. The final biomass composition trialled also represents a realistic biomass compound. However, the prediction was deemed anomalous and implausible for two out of three predictions. This result demonstrates the utility of the uncertainty threshold as despite the input representing a reasonable biomass composition, the model demonstrates high variability which should be brought to the user's attention when using the prediction.

Based on the results in Table 7, the published model contains user warnings and restrictions to prevent its misuse. Firstly, the range of capacities are limited to those used during model training (10–200 m³/h), preventing model extrapolation. Secondly, the user is warned if the prediction contains high variability i.e. the variance threshold is exceeded. Thirdly, if the variance is not exceeded, but the biomass composition is outside of the range of compositions used during training the user is warned. In both these instances the prediction is provided alongside the warning. Finally, no prediction is provided, and the user is warned if an implausible prediction is produced.

4. Study limitations

The Gibbs model is a valuable tool for simulating gasification, as it eliminates the need for defining complex equations. The model ensures that the mass and energy balance of the system is maintained, making it useful for initial process evaluations [29]. In TEA studies, the Gibbs model is widely employed to model SCWG [3–5]. One significant advantage of using the Gibbs model in an economic analysis is its ability to evaluate different feedstocks on an equivalent basis, avoiding biases that may arise from using experimental data obtained under varying conditions or levels of experimental rigour. However, it is important to note that the Gibbs reactor assumes the full conversion to gaseous products the attainment of thermodynamic equilibrium, which may not always hold true in an industrial setting. As a result, the gas composition may deviate from the predictions of the Gibbs model.

The Gibbs reactor's ability to model thermodynamic equilibrium in SCWG has been validated using high temperatures (600–900 °C) [64–67]. At elevated temperatures, reactions occur at faster rates, increasing the likelihood of attaining thermodynamic equilibrium at low residence times. A comparison between experimentally reported gas compositions and predictions from the Gibbs reactor for low-temperature SCWG (380–500 °C) are presented in Fig. S2 in the Supplementary Information. The experimental results of Louw et al. (2016), Osada et al. (2012), Yamaguchi et al. (2019), and Gökkaya Selvi et al. (2020) align reasonably well with the predictions of the Gibbs reactor [68–71]. However, the most notable deviation is observed between methane and hydrogen concentrations. This is most prominent in the results experimental by Lu et al. (2019), where significantly higher concentrations of methane and lower concentrations of hydrogen are predicted by the Gibbs model [72]. The discrepancy between hydrogen and methane concentrations has been reported previously at lower SCWG temperatures [65,66]. Higher methane formation is thermodynamically anticipated at lower temperatures owing to methanation entailing exothermic formation reactions [32,33]. As such, the differences between the Gibbs and experimental results suggest that the experimentally obtained SCWG gas compositions were not at equilibrium. To account for the assumption that thermodynamic equilibrium is obtained in this TEA study, a conservative 5-min residence time was considered for the continuous SCWG. This residence time is greater than previously investigated for continuous SCWG [2,21], and translates to an additional capital burden by oversizing the gasifier.

Table 8 – Sensitivity of the LCOH to the residence time assumed for SCWG. Biomass sample: chicken manure [73].

Processing capacity (m3/hr)	Levelised cost of hydrogen ($/kg)			
	5 min	10 min	15 min	20 min
10	14.60 (+0%)	15.64 (+7%)	16.57 (+13%)	17.43 (+19%)
20	8.21 (+0%)	9.04 (+6%)	9.80 (+11%)	10.51 (+16%)
50	4.67 (+0%)	5.33 (+5%)	5.94 (+9%)	6.52 (+13%)
100	3.55 (+0%)	4.11 (+4%)	4.65 (+8%)	5.16 (+11%)
200	3.05 (+0%)	3.55 (+3%)	4.03 (+7%)	4.50 (+10%)

As full conversion and the attainment of thermodynamic equilibrium using the assumed residence time is yet to be confirmed, a sensitivity analysis around this parameter has been conducted considering the impact of a 10, 15, and 20-min residence time on the LCOH for chicken manure [73] in the UK. The results of this analysis are presented in Table 8. A fourfold increase in residence time (20 min) led to a 10%–19% increase in the LCOH, with the greatest impact observed at the smallest processing capacity. This represents a relatively minor impact on the overall process economics and falls within the 70% probability band obtained from the Monte Carlo uncertainty analysis (+28%, on average). As such, the potential increased capital requirement to attain full conversion and thermodynamic equilibrium is comfortably captured within the considered probability band predicted by the ML surrogate model.

It is important to emphasise that the surrogate model predictions represent the economic potential of a feedstock considering full conversion to gaseous products and the attainment of thermodynamic equilibrium using continuous SCWG at 430 °C followed by SMR, HTS, and LTS. The predicted costs should therefore serve as a guide for identifying promising feedstocks based on their composition, location, and processing capacity. This allows for prioritisation of future research and development. Notably, the identification of a promising feedstock would still necessitate the optimisation of experimental conditions, i.e. residence time, catalyst type, and catalyst concentration as is undertaken in experimental studies such as [2].

5. Conclusion

A machine learning surrogate model has been created to predict the LCOH from low-temperature SCWG using different feedstock compositions, processing capacities, and geographic locations. This type of early-stage economic analysis tool helps to inform targeted research directions and investment decisions. A data-set of 600 process simulations using the Gibbs reactor provided the data to train the surrogate model. Three algorithms were investigated: RF, SVR, and ANNs. The highest prediction accuracy during cross-validation was by ANNs, achieving a test set accuracy of <4.6% (MAPE), RMSE: <0.39, and R^2: >0.99. The published surrogate model is trained on the entire dataset: doi.org/10.6084/m9.figshare.22811066.

Credit authorship contribution statement

Sarah Rodgers: Conceptualization, Data curation, Formal analysis, Investigation, Methodology, Software, Visualization, Writing – original draft, Writing – review & editing. **Alexander Bowler:** Data curation, Formal analysis, Methodology, Software, Writing – review & editing. **Jon McKechnie:** Funding acquisition, Methodology, Project administration, Resources, Supervision, Writing – review & editing. **Ed Lester:** Supervision, Writing – review & editing. **Chai Siah Lee:** Conceptualization, Methodology, Writing - review & editing. **Fanran Meng:** Methodology, Supervision, Writing – review & editing. **Laura Wells:** Methodology, Investigation, Writing – review & editing. **Martin Hayes:** Supervision, Writing – review & editing. **Stephen Poulston:** Supervision, Writing – review & editing. **Alex Conradie:** Conceptualization, Formal analysis, Funding acquisition, Methodology, Project administration, Resources, Supervision, Writing – review & editing.

Declaration of competing interest

The authors declare that they have no known competing financial interests or personal relationships that could have appeared to influence the work reported in this paper.

Acknowledgements

Appendix A. Supplementary data

Supplementary data to this article can be found online at https://doi.org/10.1016/j.ijhydene.2023.08.016.

REFERENCES

[1] Lee CS, Conradie AV, Lester E. Review of supercritical water gasification with lignocellulosic real biomass as the feedstocks: process parameters, biomass composition, catalyst development, reactor design and its challenges. Chem Eng J 2021;145:128837.

[2] Lee CS, Conradie AV, Lester E. The integration of low temperature supercritical water gasification with continuous in situ nano-catalyst synthesis for hydrogen generation from biomass wastewater. Chem Eng J 2023;445:140845.

[3] Sanaye S, Alizadeh P, Yazdani M. Thermo-economic analysis of syngas production from wet digested sewage sludge by gasification process. Renew Energy 2022;190:524—39.

[4] Liang J, Lie Y, Chen J, J E, Leng E, Zhang F, Liao G. Performance comparison of black liquor gasification and oxidation in supercritical water from thermodynamic, environmental, and techno-economic perspectives. Fuel 2023;334:126787.

[5] Okolie JA, Nanda S, Dalai AK, Kozinski JA. Techno-economic evaluation and sensitivity analysis of a conceptual design for supercritical water gasification of soybean straw to produce hydrogen. Bioresour Technol 2021;331:125005.

[6] Huntington T, Baral NR, Yang M, Sundstrom E, Scown CD. Machine learning for surrogate process models of bioproduction pathways. Bioresour Technol 2023;370:128528.

[7] Khan M, Raza Naqvi S, Ullah Z, Ali Ammar Taqvi S, Nouman Aslam Khan M, Farooq W, Taqi Mehran M, Juchelková D, Štěpanec L. Applications of machine learning in thermochemical conversion of biomass-A review. Fuel 2023;332:126055.

[8] Gopirajan PV, Gopinath KP, Sivaranjani G, Arun J. Optimization of hydrothermal gasification process through machine learning approach: experimental conditions, product yield and pollution. J Clean Prod 2021;306:127302.

[9] Li J, Pan L, Survarna M, Wang X. Machine learning aided supercritical water gasification for H2-rich syngas production with process optimization and catalyst screening. Chem Eng J 2021;426:131285.

[10] Zhao S, Jian L, Chen C, Yan B, Tao J, Chen G. Interpretable machine learning for predicting and evaluating hydrogen production via supercritical water gasification of biomass. J Clean Prod 2022;316:128244.

[11] Shenbagaraj S, Sharma Pankaj K, Sharma AK, Raghav G, Kota KB, Ashokkumar V. Gasification of food waste in supercritical water: an innovative synthesis gas composition prediction model based on Artificial Neural Networks. Int J Hydrogen Energy 2021;46(24):12739—57.

[12] Khan MNA, Haq ZU, Ullah H, Naqvi SR, Ahmed U, Zaman M, et al. Prediction of hydrogen yield from supercritical gasification process of sewage sludge using machine learning and particle swarm hybrid strategy. Int J Hydrogen Energy 2023 [in press].

[13] Fózer D, Tóth AJ, Varbanov PS, Klemeš JJ, Mizsey P. Sustainability assessment of biomethanol production via hydrothermal gasification supported by artificial neural network. J Clean Prod 2021;318:128606.

[14] Bilgiç G, Bendes E, Öztürk B, Atasever S. Recent advances in artificial neural network research for modeling hydrogen production processes. Int J Hydrogen Energy 2023;48(50):18947—77.

[15] Yahya HSM, Abbas T, Amin NAS. Optimization of hydrogen production via toluene steam reforming over Ni—Co supported modified-activated carbon using ANN coupled GA and RSM. Int J Hydrogen Energy 2021;46(48):24632—51.

[16] Kargbo HO, Zhang J, Phan AN. Robust modelling development for optimisation of hydrogen production from biomass gasification process using bootstrap aggregated neural network. Int J Hydrogen Energy 2023;48(29):10812—28.

[17] Sultana N, Hossain SMZ, Aljameel SS, Omran ME, Razzak SA, Haq B, Hossain MM. Biohydrogen from food waste: modeling and estimation by machine learning based super learner approach. Int J Hydrogen Energy 2023;48(49):18586—600.

[18] Sezer S, Özveren U. Investigation of syngas exergy value and hydrogen concentration in syngas from biomass gasification in a bubbling fluidized bed gasifier by using machine learning. Int J Hydrogen Energy 2021;46(39):20377—96.

[19] Liao M, Kelley S, Yao Y. Generating energy and Greenhouse gas inventory data of activated carbon production using machine learning and kinetic based process simulation. ACS Sustainable Chem Eng 2020;8(2):1252—61.

[20] Olafasakin O, Chang Y, Passalacqua A, Subramaniam S, Brown RC, Wright MM. Machine learning reduced order model for cost and emission assessment of a pyrolysis system. Energy Fuels 2021;35(12):9950—60.

[21] Kıpçak E, Akgün M. Biofuel production from olive mill wastewater through its Ni/Al2O3 and Ru/Al2O3 catalyzed supercritical water gasification. Renew Energy 2018;124:155—64.

[22] BEIS. Hydrogen production costs 2021, s.l. Gov.uk; 2021.

[23] Messenger, B.. Sebigas to develop 17.5 MW biogas plant to process Brazilian sugar cane waste. 2018 [Online] Available at: https://waste-management-world.com/artikel/sebigas-to-develop-175-mw-biogas-plant-to-process-brazilian-sugar-cane-waste/. [Accessed 16 December 2022].

[24] Rodgers S, Conradie A, King R, Poulston S, Hayes M, Bommareddy RR, Meng F, McKechnie J. Reconciling the sustainable manufacturing of commodity chemicals with feasible technoeconomic outcomes. Johnson Matthey Technol. Rev 2021:375—94.

[25] Pulp & Paper Canada. Hainan PM2 raises the bar for speed, water conservation. 2011 [Online] Available at: https://www.pulpandpapercanada.com/hainan-pm2-raises-the-bar-for-speed-water-conservation-1000734203/. [Accessed 7 July 2023].

[26] Kang X, Lin R, O'Shea R, Deng C, Li L, Sun Y, Murphy JD. A perspective on decarbonizing whiskey using renewable gaseous biofuel in a circular bioeconomy process. J Clean Prod 2020;255:120211.

[27] Whiskeymate. The distillery list. 2016 [Online] Available at: https://whiskymate.net/the-distillery-list/. [Accessed 22 December 2022].

[28] NNFCC. Assessment of digestate drying as an eligible heat use in the Renewable Heat Incentive. York: s.n 2016.

[29] Okolie JA, Epelle EI, Nanda S, Castello D, Dalai AK, Kozinski JA. Modeling and process optimization of hydrothermal gasification for hydrogen production: a comprehensive review. J Supercrit Fluids 2021;173:105199.

[30] Chase MW. NIST-JANAF thermochemical tables. 4th ed. New York: American Chemical Society, and the American Institute of Physics for the National Institute of Standards and Technology; 1998.

[31] Huang Y, Lo S-L. Predicting heating value of lignocellulosic biomass based on elemental analysis. Energy 2020;191:116501.

[32] Tavasoli A, Aslan A, Salimi A, Balou A, Pirbazari SM, Hashemi H, Kohansal K. Influence of the blend nickel/porous hydrothermal carbon and cattle manure hydrochar catalyst on the hydrothermal gasification of cattle manure for H2 production. Energy Convers Manag 2018;173:15—28.

[33] Hantoko D, Antoni, Kanchanatip E, Yan M, Yan, Weng Z, Gao Z, Zhong Y. Assessment of sewage sludge gasification in supercritical water for H2-rich syngas production. Process Saf Environ Protect 2019;131:63—72.

[34] Hou K, Hughes R. The kinetics of methane steam reforming over a Ni/α-Al2O catalyst. Chem Eng J 2001;82:311—28.

[35] Hla S, Park D, Duffy G, Edwards J, Roberts D, Ilyushechkin A, Morpeth L, Nguyen T. Kinetics of high-temperature water-gas shift reaction over two iron-based commercial catalysts using simulated coal-derived syngases. Chem Eng J 2009;146(1):148—54.

[36] Choi Y, Stenger H. Water gas shift reaction kinetics and reactor modeling for fuel cell garade hydrogen. J Power Sources 2003;124(2):432—9.

[37] Rodgers S, Meng F, Poulston S, Conradie A, McKechnie J. Renewable butadiene: a case for hybrid processing via bio- and chemo-catalysis. J Clean Prod 2022;364:132614.

[38] BEIS. BEIS electricity generation costs (2020). 2020 [Online] Available at: https://www.gov.uk/government/publications/beis-electricity-generation-costs-2020. [Accessed 1 February 2023].

[39] Salary Expert. Salary expert. 2022 [Online] Available at: https://www.salaryexpert.com/. [Accessed 1 December 2022].

[40] Guo H, Cui J, Li J. Biomass power generation in China: status, policies and recommendations. Biomass power generation in China: status, policies and recommendations. Energy Rep 2022;8:687–96.

[41] Renewables Now. Brazil sets price cap for May 27 auction. 2022 [Online] Available at: https://renewablesnow.com/news/brazil-sets-price-cap-for-may-27-auction-782505/. [Accessed 1 December 2022].

[42] Low Carbon Contracts Company. CfD register. 2022 [Online] Available at: https://www.lowcarboncontracts.uk/cfd-register/. [Accessed 1 December 2022].

[43] XE. Xe currency converter.. 2022 [Online] Available at: https://www.xe.com/currencyconverter/. [Accessed 12 January 2022].

[44] Kumar A, Dhall P, Kumar R. Redefining BOD:COD ratio of pulp mill industrial wastewaters in BOD analysis by formulating a specific microbial seed. Int Biodeterior Biodegrad 2010;64:197–202.

[45] EIA. Annual energy outlook 2022. Washington DC: s.n 2022.

[46] Wernet G, Bauer C, Steubing B, Reinhard J, Moreno-Ruiz E, Weidema B. The ecoinvent database version 3 (part I): overview and methodology. Int J Life Cycle Assess 2016;21:1218–30.

[47] WRAP. Digestate and compost use in agriculture. Banbury: s.n 2016.

[48] Pedregosa F, et al. Scikit-learn: machine learning in Python. J Mach Learn Res 2011;12:2825–30.

[49] Sison Arnold E, Etchieson Sydney A, Güleç Fatih, Epelle Emmanuel I, Okolie Jude A. Process modelling integrated with interpretable machine learning for predicting hydrogen and char yield during chemical looping gasification. J Clean Prod 2023;414:137579.

[50] Sinnott R, Towler G. Chemical engineering design. 5th ed. Oxford: Elsevier; 2009.

[51] WRAP. Comparing the costs of alternative waste treatment options. Banbury: WRAP; 2022.

[52] Velazquez Abad A, Dodds PE. Green hydrogen characterisation initiatives: definitions, standards, guarantees of origin, and challenges. Energy Pol 2020;138.

[53] Longden T, Beck FJ, Jotzo F, Andrews R, Prasad M. 'Clean' hydrogen? – Comparing the emissions and costs of fossil fuel versus renewable electricity based hydrogen. Appl Energy 2022;306:118145.

[54] IGES. IGES list of grid emission factors. 2022 [Online] Available at: https://www.iges.or.jp/en/pub/list-grid-emission-factor/en?_ga=2.151364921.1686382296.1673188108-667943912.1673188108. [Accessed 12 January 2023].

[55] BEIS. Government conversion factors for company reporting of greenhouse gas emissions. 2022 [Online] Available at: https://www.gov.uk/government/collections/government-conversion-factors-for-company-reporting. [Accessed 17 January 2023].

[56] Ko S, Lautala P, Handler RM. Securing the feedstock procurement for bioenergy products: a literature review on the biomass transportation and logistics. J Clean Prod 2018;200:205–18.

[57] El-Elmam RS, Özcan H. Comprehensive review on the techno-economics of sustainable large-scale clean hydrogen production. J Clean Prod 2019;220:593–609.

[58] IEA. An energy sector roadmap to carbon neutrality in China. 2021 [Online] Available at: https://www.iea.org/reports/an-energy-sector-roadmap-to-carbon-neutrality-in-china. [Accessed 8 February 2023].

[59] IEA. Opportunities for hydrogen production with CCUS in China. 2022 [Online] Available at: https://www.iea.org/reports/opportunities-for-hydrogen-production-with-ccus-in-china. [Accessed 8 February 2023].

[60] IEA. Hydrogen in Latin America. 2021 [Online] Available at: https://www.iea.org/reports/hydrogen-in-latin-america. [Accessed 8 February 2023].

[61] EIA. Natural gas. 2023 [Online] Available at: https://www.eia.gov/dnav/ng/hist/rngwhhdA.htm. [Accessed 18 March 2023].

[62] Jin B, Tan A, Liu X, Yue Y, Chen Y, Sangiovanni Vincentelli A. Using ensemble classifiers to detect incipient anomalies. Preprint 2020. https://doi.org/10.48550/arXiv.2008.08710.

[63] Ndubuaku MU, Anjum A, Liotta A. Unsupervised anomaly thresholding from reconstruction errors. In: Montella R, Ciaramella A, Fortino G, Guerrieri A, Liotta A, editors. Internet and distributed computing systems. IDCS 2019. Lecture notes in computer science. Cham: Springer; 2019. p. 123–9.

[64] Sanaye S, Alizadeh P, Yazdani M. Thermo-economic analysis of syngas production from wet digested sewage sludge by gasification process. Renew Energy 2022;190:524–39.

[65] Liang J, Liu Y, Chen J, E J, Leng E, Zhang F, Liao G. Performance comparison of black liquor gasification and oxidation in supercritical water from thermodynamic, environmental, and techno-economic perspectives. Fuel 2023;334:126787.

[66] Qian L, Wang S, Wang S, Zhao S, Zhang B. Supercritical water gasification and partial oxidation of municipal sewage sludge: an experimental and thermodynamic study. Int J Hydrogen Energy 2021;46(1):89–99.

[67] Louw J, Schwarz CE, Knoetze JH, Burger AJ. Thermodynamic modelling of supercritical water gasification: investigating the effect of biomass composition to aid in the selection of appropriate feedstock material. Bioresour Technol 2014;174:11–23.

[68] Louw J, Schwarz CE, Burger AJ. Catalytic supercritical water gasification of primary paper sludge using a homogeneous and heterogeneous catalyst: experimental vs thermodynamic equilibrium results. Bioresour Technol 2016:111–20.

[69] Osada M, Yamaguchi A, Hiyoshi N, Sato O, Shirai M. Gasification of sugarcane bagasse over supported ruthenium catalysts in supercritical water. ENERG FUEL 2012;26(6):31179–3186.

[70] Yamaguchi A, Watanabe T, Saito K, Kuwano S, Murakami Y, Mimura N, Sato O. Direct conversion of lignocellulosic biomass into aromatic monomers over supported metal catalysts in supercritical water. Mol Catal 2019;477.

[71] Gökkaya Selvi D, et al. Hydrothermal gasification of the isolated hemicellulose and sawdust of the white poplar (Populus alba L.). J Supercrit Fluids 2020;162.

[72] Lu Y, Jin H, Zhang R. Evaluation of stability and catalytic activity of Ni catalysts for hydrogen production by biomass gasification in supercritical water. Carbon Resour. Convers. 2019:95–101.

[73] Babaei K, Bozorg A, Tavasoli A. Hydrogen-rich gas production through supercritical water gasification of chicken manure over activated carbon/ceria-based nickel catalysts. J Anal Appl Pyrolysis 2021;159:105318.